Coupled semiconductor lasers and their applications in telecommunications and networks

Michail Bourmpos*

National and Kapodistrian University of Athens
Department of Informatics and Telecommunications
mmpour@di.uoa.gr

Abstract. The aim of this thesis is to theoretically and experimentally investigate the nonlinear dynamics of coupled semiconductor lasers, in various network topologies and under different operating conditions. The nodes of the aforementioned networks proved capable of exhibiting synchronized chaotic optical outputs and in special cases at zero-lag. The first large scale network implementation of bidirectionally coupled semiconductor lasers with long interacting cavities, is presented.

1. Introduction

Coupled oscillators are capable of producing diverse dynamics and therefore have been a topic of great interest, with many applications in fields such as cryptography [1], telecommunications [2], control engineering [3] and more. The collective behavior of coupled oscillators, in various network topologies, has also been investigated over the past decades, driven mainly by the fact that these networks can be directly associated with complex physical [4] or biological systems [5]. Semiconductor lasers (SLs) are known nonlinear elements that generate complex dynamics and have been extensively used as models in the aforementioned networks [6]. In the simplest case of a mutual interacting network, two mutually coupled identical SLs can produce generalized synchronized dynamics [7]. When a third - relay element is added between them, isochronous synchronization can be achieved [8]. Zero-lag synchronization has also been observed for larger networks with multiple nodes [6]. In the present work, we have investigated arithmetically and experimentally multi-nodal all-optical networks in various topologies based on mutual coupling, in terms of synchronization, complexity and robustness. The nodes are represented by typical semiconductor lasers.

The rate equation mathematical model has been used to describe the operation and dynamics of the nodes, which can be applied to any of the investigated network topologies. This model is formulated in vector form and is based on the Lang Kobayashi model [9], originating from the representation used in [6] and including frequency detuning terms among oscillators as in [10].

$$\frac{d\vec{E}(t)}{dt} = j\overrightarrow{\Delta\omega} \circ \vec{E}(t) + \frac{1}{2}(1+j\alpha)\left(\vec{G}(t) - \frac{1}{t_{ph}}\right) \circ \vec{E}(t)$$
$$+ \mathbf{K^T}\left(\vec{E}(t-\tau)\right) \circ e^{-j\omega_0\tau} + \sqrt{\mathbf{D}}\,\vec{\xi}(t) \tag{1}$$

$$\frac{d\vec{N}(t)}{dt} = \frac{\vec{I}}{e} - \frac{\vec{N}(t)}{t_s} - \vec{G}(t) \circ \left|\vec{E}(t)\right|^2 \tag{2}$$

$$\vec{G}(t) = g_n\left(\vec{N}(t) - N_0\right) \circ \left(1 + s\left|\vec{E}(t)\right|^2\right)^{\circ -1} \tag{3}$$

The vectors of the SLs optical fields and carrier densities are $\vec{E}(t)=[E_1(t);E_2(t); ... ;E_n(t)]$ and $\vec{N}(t)=[N_1(t);N_2(t); ... ;N_n(t)]$ respectively. The vector of uncorrelated complex Gaussian white noises is represented by $\vec{\xi}(t)$. The time delays and

---

* Dissertation Advisor: Professor Dimitris Syvridis

couplings between the nodes of the network are kept in the n x n arrays K and τ, where the actual values from node i to node j are represented as τ_{ij} and k_{ij} respectively. By appropriate manipulation of the coupling and time delay arrays (K and τ) we can construct the desired network topologies, adopting coupling asymmetries wherever needed. The result of the Hadamard product ($\circ$) between the n x n arrays of the time delayed optical field $E(t\text{-}\tau)$ and the phase shift $e^{-j\omega_0\tau}$ in equation (1), is also a n x n array, where the element (i,j) is the delayed optical field of i injected into j, followed by the corresponding phase shift, thus equal to $E_i(t - \tau_{ij})e^{-j\omega_0\tau_{ij}}$. Vector $\vec{I}$ of equation (2) contains the biasing current for all lasers which is set to $I=18mA$ throughout this work, while the solitary lasing emission threshold is $I_{th}=17.4mA$. Each laser is detuned with respect to the reference laser frequency ω_0, at variable values $\Delta\omega_j$, included in the vector $\overrightarrow{\Delta\omega}$ of equation (1). The n x 1 vectors α, t_{ph} and s, include the linewidth enhancement factors, photon lifetimes and saturation gain coefficients of the n SLs respectively. Finally, vector $\left|\vec{E}(t)\right|^2 = [|E_1(t)|^2 |E_2(t)|^2 \dots |E_n(t)|^2]$ contains the power of optical fields. The Hadamard inverse $(1 + s \circ \left|\vec{E}(t)\right|^2)^{\circ-1}$ yields $1/(1 + s_i|E_i(t)|^2)$ for the i_{th} laser. SLs share the same values for the rest of their intrinsic parameters, so there parameters g_n and N_0 are not expressed in vector form, although this could also be possible.

Simulations were performed for the set of differential equations (1-3) using the 4th order Runge-Kutta method, with a time-step of 0.8psec. Optical power has been deducted from the complex optical field using the appropriate conversion [11].

In all network topologies presented below, we formulate the coupling matrix K and assume that the time delay matrix is similarly constructed, with constant values of *5ns* delays between the nodes. The frequency detuning from the reference laser frequency are randomly chosen, following a Gaussian distribution in the range of $2\pi\cdot(\pm1GHz)$.

2. Star Network

For a star network of 50 remote nodes coupled through a central typical SL we formulate the 51x51 coupling matrix K as follows:

$$K = \begin{bmatrix} 0 & 0 & \dots & 0 & k_{1,51} \\ 0 & 0 & \dots & 0 & k_{2,51} \\ \vdots & \vdots & \vdots & \vdots & \vdots \\ 0 & 0 & \dots & 0 & k_{50,51} \\ k_{51,1} & k_{51,2} & \dots & k_{51,50} & 0 \end{bmatrix} \qquad (4)$$

The 51st row of the matrix is matched with the central node of the star topology. We have assumed identical couplings from the hub node to the star nodes ($k_{51,i} = k_{51,j} = k$) and from star nodes to the hub $k_{i,51} = k_{j,51} = \beta \cdot k$, where *0<β<1* is a coupling asymmetry coefficient we have introduced to keep the accumulated optical injection into the hub laser within reasonable range.

We must point out that for this topology the hub laser frequency detuning is assumed to be zero, without loss of generality.

For different values of the parameter pair *(k,β)*, a mapping of the mean zero-lag cross-correlation between all SL pairs *(i,j)* is constructed, as shown in figure 1.

Based on this mapping, we have selected the pair of parameters *{k=60ns^{-1}, β=0.5}* where high zero-lag mean cross-correlation is achieved ($C_{i,j}^{mean}$=0.921) in combination with higher complexity. For this pair of values, a sensitivity analysis, when a SL is added or subtracted from the network, is performed.

First we connect a new node to the network, with various coupling and time-delay parameter values. We are interested in whether the connection of this non-identical laser with unmatched operational parameters will influence the behaviour of the backbone network. Moreover, we would like to know the tolerance in the parameter mismatch in order for the SL to be synchronized with the rest of the nodes in the network and if this node-addition can somehow be detected.
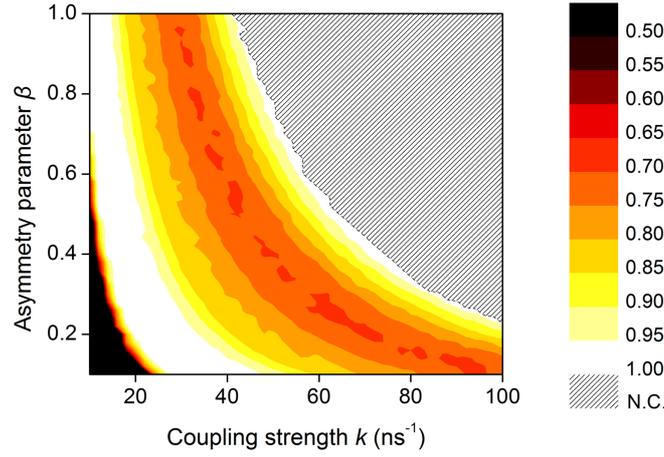
Figure 1. Mean zero-lag cross-correlation among the 50 star lasers.

For various values in the frequency detuning of the newly connected node and its time delay from the hub laser we calculate the change in the mean and minimum (worst case) zero-lag cross correlation of the original 50-node star network (figure 2).

It is evident that the network has absorbed the mismatch of the one additional laser, even if its detuning is significantly larger than 1GHz or its time-delay is different than *5ns*. The difference in the mean and minimum zero-lag cross-correlation is statistical and calculated to be $|\Delta C_{i,j}^{mean}|$~*0.013* and $|\Delta C_{i,j}^{min}|$~*0.021* respectively. The only parameter values of the added node for which the change is not statistical lie in the region of *τ=5ns* and for small frequency detuning values. The consistence of these values with the rest of the network parameters imposes a measurable positive change in the mean correlation value, making the synchronized new node detectable by the network.

Disconnecting a SL from the original network of 50 nodes is a rather more straightforward case. The mean correlation of the network after disconnecting the new laser is shifted now to a lower value by $\Delta C_{i,j}^{mean}$ = *-0.012*, attributed to a reduction of the coupling strength among the 49 lasers left within the network. However, simulation results prove that there is no dependence on the value of the disconnected laser's frequency detuning; the effect of disconnecting a node with large detuning seems almost equivalent to disconnecting a node with close to zero detuning.
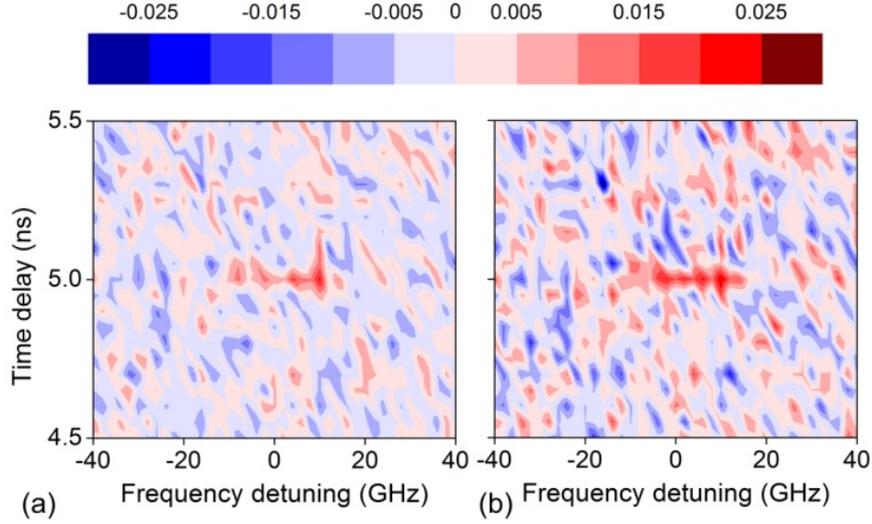
Figure 2. Change in the mean (a) and minimum (b) zero-lag cross correlation of the 50 star laser network, when an additional laser is connected to the network, for various values of frequency detuning and time delay of the added laser.

3. Mesh Network

For a fully-connected mesh network of 50 SLs, each one coupled to every other, we formulate the 50x50 coupling matrix K as follows:

$$K = \begin{bmatrix} k_{1,1} & k_{1,2} & ... & k_{1,49} & k_{1,50} \\ k_{2,1} & k_{2,2} & ... & k_{2,49} & k_{2,50} \\ \vdots & \vdots & \vdots & \vdots & \vdots \\ k_{49,1} & k_{49,2} & ... & k_{49,49} & k_{49,50} \\ k_{50,1} & k_{50,2} & ... & k_{50,49} & k_{50,50} \end{bmatrix} \tag{5}$$

where $k_{i,i}=0$ for zero feedback of the SL nodes.

Assuming equal couplings $k_{i,j}=k,\ \forall i,j$ and for different values of k we plot the mean zero-lag cross-correlation between all SL pairs (figure 3). Based on this figure we choose $k=1.5ns^{-1}$ as the coupling between the nodes, which yields a mean zero-lag cross-correlation of $C_{i,j}^{mean}=0.964$ and then add a new node, with different parameter values, to the network.

Again, the network has absorbed the mismatch of the one additional laser (figure 4). The difference in the mean and minimum zero-lag cross-correlation is statistical and calculated to be $|\Delta C_{i,j}^{mean}|\sim 0.001$ and $|\Delta C_{i,j}^{min}|\sim 0.004$ respectively. The newly added SL produces a consistent, non-statistical increase in the mean and minimum zero-lag cross-correlation of the network, only when it's time-delay is equal to *5ns* - the common time-delay of all nodes - and for small values of frequency detuning. Similar results to those of the star network are obtained for the maximum value of the mean cross-correlation between the connected laser and the 50 SLs in the fully-connected mesh network, as well as for the corresponding time-lag, for various detuning and time delay values of the added node.

Disconnecting a node from the network leads to a detectable minor mean cross-correlation degradation, which is statistical and independent of the removed node's frequency detuning, as in the case of the star network.
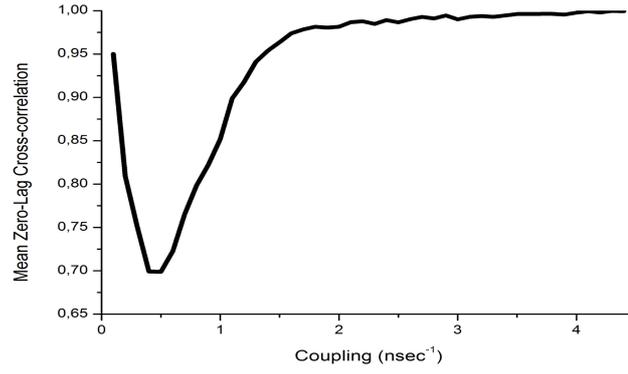
Figure 3. Mean zero-lag cross-correlation among the 50 star lasers.
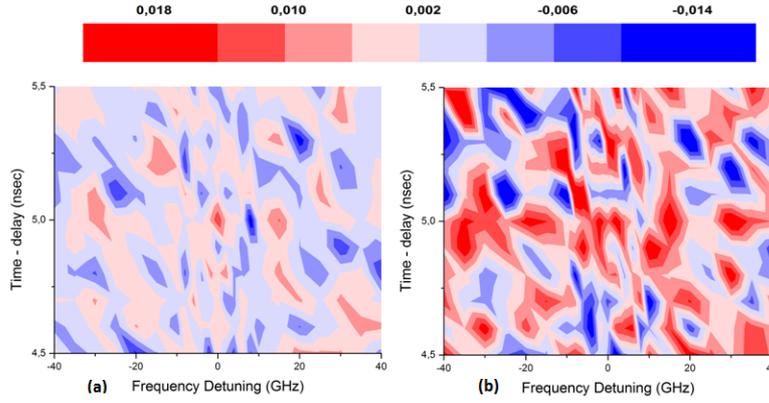
Figure 4. Change in the mean (a) and minimum (b) zero-lag cross correlation of the 50 laser fully-connected mesh network, when an additional laser is connected to the network, for various values of frequency detuning and time delay of the added laser.

4. Ring Network

For a ring network of 50 SLs, where every node is connected only to its two neighbors, the 50x50 coupling matrix K is formulated as follows:

$$K = \begin{bmatrix} k_{1,1} & k_{1,2} & 0 & ... & 0 & 0 & k_{1,50} \\ k_{2,1} & k_{2,2} & k_{2,3} & ... & 0 & 0 & 0 \\ 0 & k_{3,2} & k_{3,3} & ... & 0 & 0 & 0 \\ \vdots & \vdots & \vdots & \vdots & \vdots & \vdots & \vdots \\ 0 & 0 & 0 & ... & k_{48,48} & k_{48,49} & 0 \\ 0 & 0 & 0 & ... & k_{49,48} & k_{49,49} & k_{49,50} \\ k_{50,1} & 0 & 0 & ... & 0 & k_{50,49} & k_{50,50} \end{bmatrix} \qquad (6)$$

with $k_{i,i}=0$ for zero feedback of the SL nodes, common couplings $k_{i,j}=k,\ \forall i,j$ and time delays of *5ns.* The nodes are sorted and positioned in the ring by increasing frequency detuning values.

For different coupling values we calculate the maximum cross-correlation between all node-pairs and the corresponding lag. Only the second nearest neighbors (i-2 and i+2 for the ith node) have consistently their maximum cross-correlation value at zero lag, even though this is also observed in several other 'even pairs' (j with j+2·l). We plot (figure 5) the maximum, mean and minimum of these cross-correlation (regardless of lag) values. Only for small couplings, where low complexity dynamics are observed, we obtain high cross-correlation values.

Ring network topologies exhibit poor synchronization quality and thus are of no particular interest regarding possible application in telecommunications or sensing.
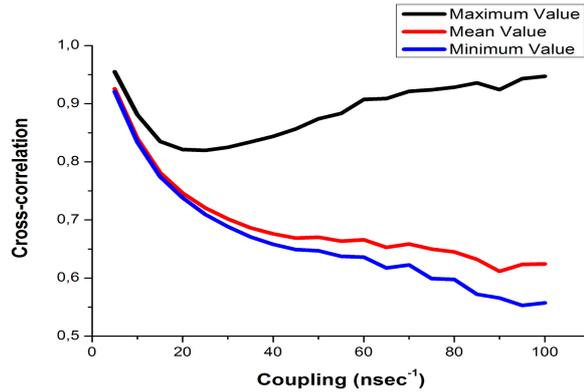
Figure 5. Maximum, mean and minimum cross correlation of all pairs in the 50 node fully-connected mesh network, regardless of lag.

5. Effect of parameters on synchronization

We have also investigated two different mutually coupled SL network topologies, with respect to the number of nodes and the discrepancies in key SL parameters. Star or fully-connected mesh networks with M=8, 16 and 24 nodes seem to be significantly affected by the differences in the SLs linewidth enhancement factor and photon life time parameters. The wider the range these different values are spread, the worse the efficiency of the synchronized dynamics. The same applies for discrepancies in the operating frequency of the SLs, as also shown in previous research. Differences in the saturation gain coefficient are unimportant as proven in this work. Furthermore, the full-mesh network topology seems to better cope with parameter mismatch, than the star network topology. Based on the above, we can propose that the full-mesh network topology should be adopted for a large-scale experiment of optical networks yielding synchronized complex dynamics. Given that the operating frequency can be adjusted by use of temperature control, it seems of the outmost importance to be able to manufacture and use SLs with similar intrinsic parameter values, especially for the linewidth enhancement factor and the photon life time, which have been proven to be of significance.

6. Bubbling

Differences in the internal characteristics of the SL nodes have a noteworthy impact on the performance and quality of network synchronization. For instance, networks with small differences in the SLs free-running frequencies require larger coupling strengths and/or smaller driving currents for adequate synchronization of the produced signals. In any case, de-synchronization windows of rather small duration - even at well-synchronized systems - have been observed. These intermittent de-

synchronizations are noise and/or parameter mismatch induced events, referred in literature also as bubbling [12,13]. They have been observed both as fast and frequent events in the coherence-collapse regime and as slower and less-frequent events in the low-frequency fluctuation (LFF) regime, in the case of bi-directionally coupled SLs [12,13].

In this work we have numerically investigated the behavior of bubbling effects in a well-synchronized SL network, adopting a star topology, and how these events determine the network's overall operation. We have concentrated on cases where chaotic dynamics are generated under strong node coupling. Zero-lag cross-correlation and synchronization error between pairs of star nodes in this network are estimated, for various conditions of delay between nodes, coupling strength and driving current of the mediating element (hub). In the context of these investigations, the statistical properties of the de-synchronization events are monitored and quantified, such as their reproducibility and duration. The general trends of bubbling statistics are finally associated with the physical phenomena caused by the changes in the network's critical variables.

The behavior of a star SL network has been examined, while altering certain key network parameters in terms of the de-synchronization events that appear in well-synchronized chaotic dynamics. Longer links between the star and hub nodes lead to longer and more infrequent de-synchronization events, keeping the overall synchronization at almost the same levels. On the contrary, the increase in coupling strengths leads to a more efficient synchronization with shorter and more infrequent bubbling events. Finally, the increase in the hub SLs driving current eventually leads to minimization or even elimination of the de-synchronization events by upgrading the role of the hub in the network operation, and interchanging its lagging with leading dynamics.

7. Experimental investigation

In the present work we have extended the generalized synchrony investigations in a network of up to 16 mutually-coupled identical SLs, connected through similar - yet unmatched - distant optical paths. We show that each unit's properties and operating parameters establish it as a member of the overall synchronized network, a member of intra-network synchronized clusters or just an outlier unit. Strict frequency matching (<200MHz) of the optical emitted signals allow synchrony at configurations with even a few identical SLs. In contrast, when non-identical SLs couple with the network they fail to synchronize at any operational condition. Moreover, when shifting identical SLs from a common emission wavelength (global operation) to multiplexed wavelengths (cluster operation), it is shown that the network can maintain intra-cluster synchrony. The latter property is validated for ultra-dense wavelength multiplexing of the coupled units, with chaotic carrier spectral distance of only 50pm.

The coupling topology follows the fully-connected SL architecture shown in figure 6a. Each laser is selected from a pool of identical SLs and emits to the network, while receiving from all counterparts - including its own signal - through a common tunable reflector. For up to 16 lasers (or else referred as network nodes) and no long-haul transmission path, one amplification stage provides sufficient power to the injected signals for laser synchrony. However, in the presented investigation two amplification stages are used so that a larger range of coupling strengths can be tested among the laser nodes. Optical filtering with 0.36nm (~40GHz) 3dB-bandwidth is used to reduce erbium-doped fiber amplifiers' (EDFA) spontaneous emission, without imposing frequency-selective feedback conditions. Inline fiber

power monitors (PM) display the circulating average optical power. The total round trip time of the cavities formed between pairs of lasers is 117.92 ± 0.12m. Each laser's optical output is monitored through isolated ports that eliminate any residual feedback. These outputs are used to screen the optical and microwave properties of the emitted signals through appropriate monitoring instrumentation.
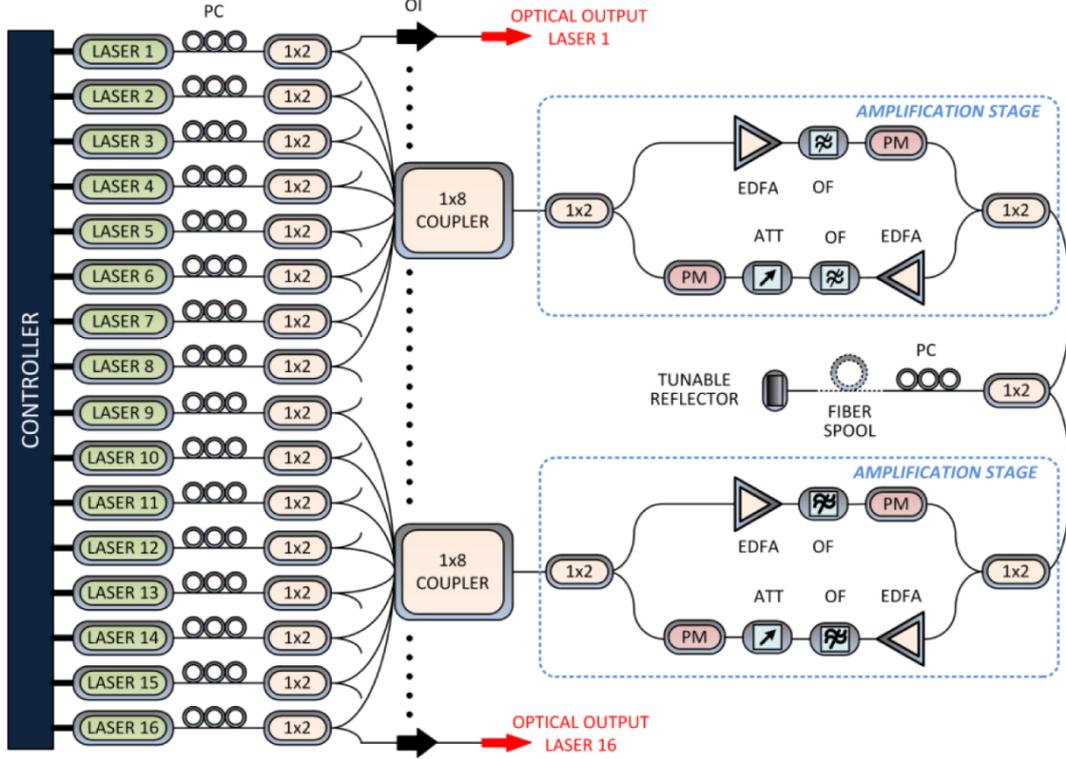
Figure 6. Full-mesh-type network with optically-coupled 16 SLs. Laser network topology: PC: Polarization controller, 1x2 and 1x8: optical couplers, EDFA: 25dB-gain Erbium-doped fiber amplifier, OF: Optical filter, PM: Inline optical power monitor, ATT: Optical attenuator.

The coupling strength among the SLs determines not only the synchrony performance but also shapes the emitted laser dynamics through which synchrony is achieved. The injection ratio $R^{L\#}$ is a measure of the coupling strength among the SLs and expresses the ratio of the optical power inserted into a laser divided by the optical power emitted by the same laser. Thus, for a given laser $L_\#$ that participates in the coupled network, it is defined as:

$$R^{L\#} = C^2 \cdot \frac{P_{inj}^{tot}}{P_{em}^{L\#}} \tag{7}$$

where C is the laser-fiber coupling loss, P_{inj}^{tot} is the total optical power reaching laser $L_\#$ through the associated fiber path and $P_{em}^{L\#}$ is the optical emitted power of laser $L_\#$ measured at its output fiber tip. Coupling loss C between laser facet and fiber is a parameter which cannot be verified directly for each device, since all devices are fiber pigtailed. For the injection ratio estimation, a value of $C = 0.5$ is used for all lasers, according to the specifications given by the laser manufacturer.

As presented in figure 7, optical coupling affects signal emission from very low R values (as low as 0.001), forcing the 16 lasers to deviate from the continuous wave emission and oscillate in various dynamical states. Only when $R>0.05$ correlated chaotic emission for the overall network (*average-CC*>0.8) is observed among all coupled lasers (gray-marked region). Even slight mismatches in SLs'

internal parameters, operational characteristics, optical emission frequencies, as well as small deviations from polarization alignment, may result in different levels of synchrony. In the example of figure 7, the laser pair $L_{\#1}$ - $L_{\#2}$ shows an *average-CC* above 0.93, while the laser pair $L_{\#6}$-$L_{\#7}$ shows an *average-CC* close to 0.86. The variance of each *average-CC* value is explained by the transversal instabilities of the synchronization manifold imposed by the overall network operation. The appearance of de-synchronization events, albeit always present, shows a dependence on the coupling strength among the laser nodes. Their duration and occurrence frequency shape the correlation and variance level for each coupling strength condition. In figure 8 such de-synchronization events are shown between two SLs ($L_{\#1}$ and $L_{\#2}$) emissions. Usually when power dropouts arise in the emitted dynamics, de-synchronization for a small period of time - of the order of ns - is present. The fact that this duration is significantly shorter than the period for which the two lasers preserve high-level of synchronization deems the change in the statistical metric of *averaged-CC* insignificant. This behavior refers to an optimally coupled and operated 16-SL network. If SLs are biased to favor LFF emission or unmatched operational conditions apply, the de-synchronization events last longer, affecting the overall synchronization level. Finally, for very strong injection ratios (above 1), increased instabilities are observed, accompanied by longer de-synchronization events or lower complexity attractors, periodic oscillations and even continuous wave operation.
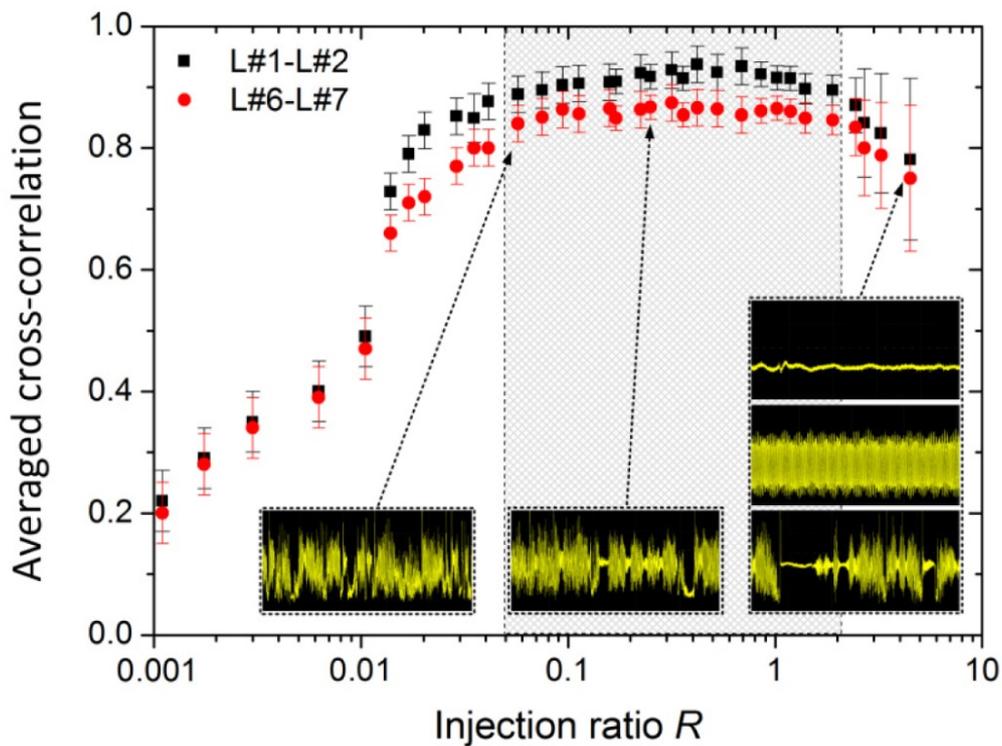
Figure 7. Effect of coupling strength on the correlated emission of a 16-laser coupled network. *Averaged-CC* values between two pairs of SLs (*L#1-L#2* and *L#6-L#7*) vs. the applied injection ratio, when the emitted power from the lasers is set to −15dBm. Timetraces in insets show the dynamics of the emitted signals for different coupling strengths. Gray region indicates synchronized network coupling conditions through chaotic signals
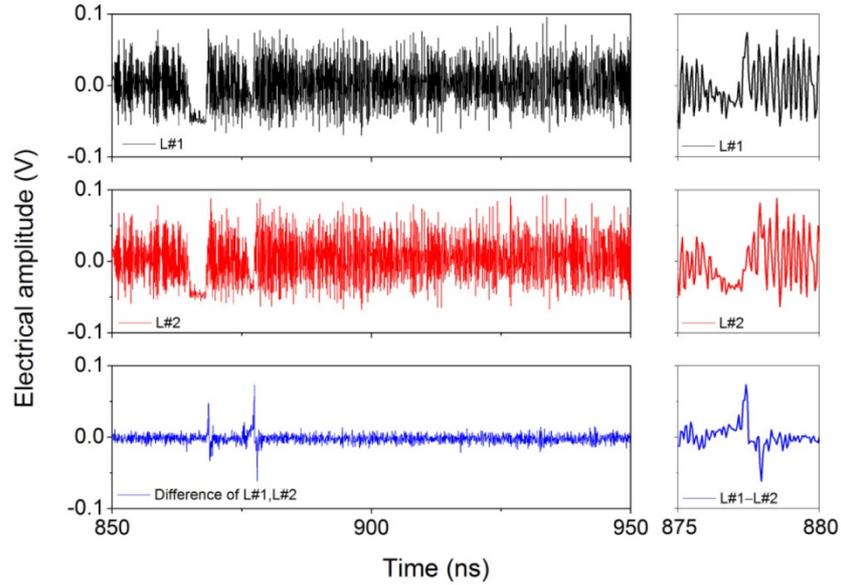
Figure 8. Temporal evolution of *L#1* and *L#2* emission, as well as their difference in a coupled 16-laser network, when R = 0.2dB. De-synchronization events appear when power dropouts occur and are minimized for optimal operating and coupling conditions. In the right column, a detail in the temporal region where a de-synchronization event takes place is provided.

8. Applications

Security

The concept of security in a 8-SLs network is tested by substituting one SL with a device provided from another manufacturer. In this investigation we study the potential of a user optically coupling with the network with a non-identical SL device to synchronize.

Wavelength emission is matched among all SLs, while the biasing current of the different SL and the optical injection level are varied so as to achieve the best synchrony level within the network. When considering moderate optical coupling (R = −9dB), the highest achieved *averaged-CC* between the non-identical SL and any of the identical SLs group is 0.34 at its most, as shown in figure 9a. It is obtained for the non-identical SL's near-threshold operation and is greatly lower than the worst synchronized pair within the identical SLs group (*averaged-CC*~0.82).

By enhancing the coupling conditions to R = −0.5dB, as presented in figure 9b, an equivalent behavior is observed. The only difference observed is the improved values of *averaged-CC* for the different (~0.62) and same manufacturers' (~0.89) SLs. Consequently, dissimilar hardware SL units hold by unauthenticated users fail to synchronize with the network at any operational condition. On the other hand, users with identical devices can access synchronized emission, as long as they select matched operating conditions and same dynamical regimes. Equivalent findings are also validated for a network containing two out of eight SLs from a different manufacturer.
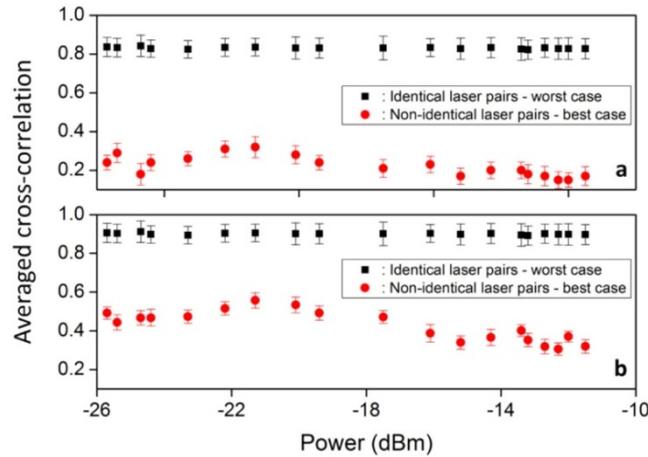
Figure 9. Synchrony comparison in an 8-node coupled network that includes 7 identical SLs and 1 SL from a different manufacturer. The comparison is made between the worst performance among the 7 identical lasers (black rectangles) and the best performance of synchronization between the different SL and the 7 identical lasers (red circles), versus the different SL's emitted optical power and for (a) $R = −9$dBm and (b) $R = −0.5$dBm. All uncoupled identical lasers emit optical power $−15$dBm, while all uncoupled lasers operate at $\lambda = 1549.600$nm

Clustering

In a smaller network, we optically couple 8 SLs and examine the potential of the network SL nodes to obtain cluster synchrony by imposing frequency emission grouping. Initially, for small frequency detuning (<200MHz) of all 8 SLs - as in the 16-laser network case - optimized conditions lead to highly correlated emission. Specifically, pairwise *averaged-CC* values of at least 0.88, and as high as 0.97, are recorded for full-bandwidth detected signals, as shown in figure 10a. It becomes clear that by controlling frequency-matching conditions we can drastically reduce the least number of coupled nodes required for synchronized operation. By thermally shifting the emission wavelengths of the second quartet of lasers ($L_{\#5}$-$L_{\#8}$) by 50pm we obtain the correlation mapping if figure 10b. Synchrony is observed between lasers that participate in each cluster ($L_{\#1}$-$L_{\#4}$ and $L_{\#5}$-$L_{\#8}$) while correlated emission is always at very low levels when comparing inter-cluster nodes (*averaged-CC*<0.61). Thus, the same configuration can also lead to cluster synchronization.
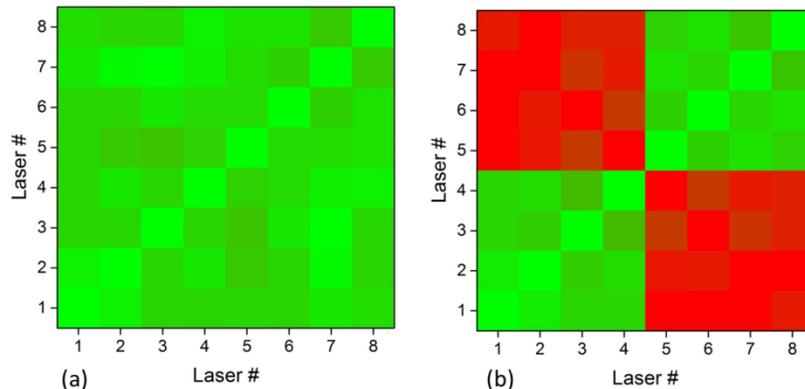
Figure 10. Cluster synchronization in an 8-SL coupled network configuration. Cross-correlation mapping with (a) zero-detuned wavelength laser emission, and (b) with cluster synchronization among two quartets of lasers ($L_{\#1}$-$L_{\#4}$ and $L_{\#5}$-$L_{\#8}$) that are 50pm spaced in wavelength.

9. Conclusions

In the present work, we have arithmetically and experimentally investigated multi-nodal all-optical networks, in various topologies and in terms of synchronization, complexity and robustness. We have presented the first large-scale implementation of 16 optically coupled and independently controlled SLs in a fully-connected synchronized network topology. The overall consistency of the synchronized network is profound albeit the presence of mismatched or disparate lasers interacting through optical coupling. Local instabilities causing short de-synchronization events do not annihilate the overall high level of synchrony.

Our work can be the basis on which advanced sensing and authentication protocols in future fiber-optic networks can be proposed. In an envisaged application based on the concept of this work, other real-life large-scale networks of coupled oscillators can be simulated through the use of SLs, exploiting the speed of phenomena evolution in such configurations, for prediction purposes.

REFERENCES

[1] Uchida, A.,, Amano, K., Inoue, M., Hirano, K., Naito, S., Someya, H., Oowada, I., Kurashige, Y., Shiki, M., Yoshimori, S., Yoshimura, K., and Davis, P., "Fast physical random bit generation with chaotic semiconductor lasers," Nat. Phot. 2, 728–732 (2008).

[2] Argyris, A., Syvridis, D., Larger, L., Annovazzi-Lodi, V., Colet, P., Fischer, I., García-Ojalvo, J., Mirasso, C.R., Pesquera, L., and Shore, K.A., "Chaos-based communications at high bit rates using commercial fiber-optic links," Nature 438 (7066), 343-346, (2005).

[3] Fradkov, A.L., Evans, R.J., and Andrievsky, B.R., "Control of chaos: methods and applications in mechanics," Phil. Trans. R. Soc. A 364, 2279-2307 (2006).

[4] Strogatz, S.H., Abrams, D.M., McRobie, A., Eckhardt, B., and Ott, E., "Crowd synchrony on the millennium bridge," Nature 438 (7064), 43-44 (2005)

[5] Strogatz, S.H., and Stewart, I., "Coupled oscillators and biological synchronization,", Scient. Amer. 269, 68–73 (1993).

[6] Zamora-Munt, J. , Masoller, C., Garcia-Ojalvo, J. and Roy R., "Crowd synchrony and quorum sensing in delay-coupled lasers," Phys. Rev. Lett. 105, 264101 (2010).

[7] Mulet, J., Mirasso, C.R., Heil, T., and Fischer I., "Synchronization scenario of two distant mutually coupled semiconductor lasers", J. Opt. B: Quantum Sem. Opt. 6, 97 (2004).

[8] Zhou, B.B., and Roy R., "Isochronal synchrony and bidirectionalcommunication with delay-coupled nonlinear oscillators", Phys. Rev. E 75, 026205 (2007).

[9] Lang, R., and Kobayashi, K., "External optical feedback effects on semiconductor injection laser properties," IEEE J. Quantum Electron. 16, 347-355 (1980).

[10] Fischer, I., Vicente, R., Buldú, J.M., Peil, M., Mirasso, C.R., Torrent, M.C., and García-Ojalvo, J., "Zero-Lag Long-Range Synchronization via Dynamical Relaying," Phys. Rev. Lett. 97, 123902 (2006).

[11] Petermann, K. [Laser Diode Modulation And Noise], New Ed. Kluwer Academic Publishers Group, Netherlands (1991).

[12] J. Tiana-Alsina, K. Hicke, X. Porte, M. C. Soriano, M. C. Torrent, J. Garcia-Ojalvo and I. Fischer, "Zero-lag synchronization and bubbling in delay-coupled lasers", *Phys. Rev. E* vol. 85, 026209, 2012.

[13] V. Flunkert, O. D'Huys, J. Danckaert, I. Fischer, and E. Schöll, "Bubbling in delay-coupled lasers", *Phys. Rev. E* vol. 79, 065201, 2009.